Yeast Rgd3 is a phospho-regulated F-BAR–containing RhoGAP involved in the regulation of Rho3 distribution and cell morphology

Robert M. Gingras, Kyaw Myo Lwin†, Abigail M. Miller, and Anthony Bretscher*
Department of Molecular Biology and Genetics, Weill Institute for Cell and Molecular Biology, Cornell University, Ithaca, NY 14853

ABSTRACT **Polarized growth requires the integration of polarity pathways with the delivery of exocytic vesicles for cell expansion and counterbalancing endocytic uptake. In budding yeast, the myosin-V Myo2 is aided by the kinesin-related protein Smy1 in carrying out the essential Sec4-dependent transport of secretory vesicles to sites of polarized growth. Overexpression suppressors of a conditional *myo2 smy1* mutant identified a novel F-BAR (Fes/CIP4 homology-Bin-Amphiphysin-Rvs protein)-containing RhoGAP, Rgd3, that has activity primarily on Rho3, but also Cdc42. Internally tagged Rho3 is restricted to the plasma membrane in a gradient corresponding to cell polarity that is altered upon Rgd3 overexpression. Rgd3 itself is localized to dynamic polarized vesicles that, while distinct from constitutive secretory vesicles, are dependent on actin and Myo2 function. In vitro Rgd3 associates with liposomes in a PIP_2-enhanced manner. Further, the Rgd3 C-terminal region contains several phosphorylatable residues within a reported SH3-binding motif. An unphosphorylated mimetic construct is active and highly polarized, while the phospho-mimetic form is not. Rgd3 is capable of activating Myo2, dependent on its phospho state, and Rgd3 overexpression rescues aberrant Rho3 localization and cell morphologies seen at the restrictive temperature in the *myo2 smy1* mutant. We propose a model where Rgd3 functions to modulate and maintain Rho3 polarity during growth.**

Monitoring Editor
Rong Li
Johns Hopkins University and National University of Singapore

Received: May 6, 2020
Revised: Sep 3, 2020
Accepted: Sep 9, 2020

INTRODUCTION

Budding yeast grows in a polarized manner with the cell selecting one site for bud emergence, followed by bud growth, organelle segregation, and ultimately cytokinesis. Achieving polarized growth requires the integration of signaling pathways and the assembly of a polarized cytoskeleton that guides membrane and organelle transport. In budding yeast, the microtubule cytoskeleton is responsible for nuclear orientation and mitosis, and the actin-based cytoskeleton is used for the transport and segregation of organelles, endocytosis, and the contractile ring during cytokinesis (reviewed in Schott *et al.*, 2002).

The transport of post-Golgi secretory vesicles and segregation of all organelles is dependent on the assembly of actin cables at the bud cortex and bud neck by the two formins, Bni1 and Bnr1, respectively. These cables serve as tracks for the two myosin-V motors in yeast, the essential Myo2 that transports secretory vesicles, mitochondria, peroxisomes, the vacuole, and the cytoplasmic microtubules for nuclear orientation and Myo4 that transports mRNAs and the endoplasmic reticulum. Myo2 is a typical myosin-V heavy chain consisting of an N-terminal motor domain followed by IQ-motif repeats and a coiled-coil dimerization domain and terminating in a large globular cargo-binding tail domain. The tail domain associates with organelle-specific receptors to mediate their transport. Here it associates with the Rab protein Sec4 for transport of secretory vesicles, Mmr1 and Ypt11 for mitochondrial transport, Inp2 for peroxisome transport, Vac17 for

This article was published online ahead of print in MBoC in Press (http://www.molbiolcell.org/cgi/doi/10.1091/mbc.E20-05-0288) on September 17, 2020.

†Present address: Department of Structural Biology, Rockefeller University, New York, NY 10065.

*Address correspondence to: Anthony Bretscher (apb5@cornell.edu).

Abbreviations used: F-BAR, Fes/CIP4 homology-Bin-Amphiphysin-Rvs protein; GAP, GTPase-activating protein; imNG, internal-mNeonGreen.

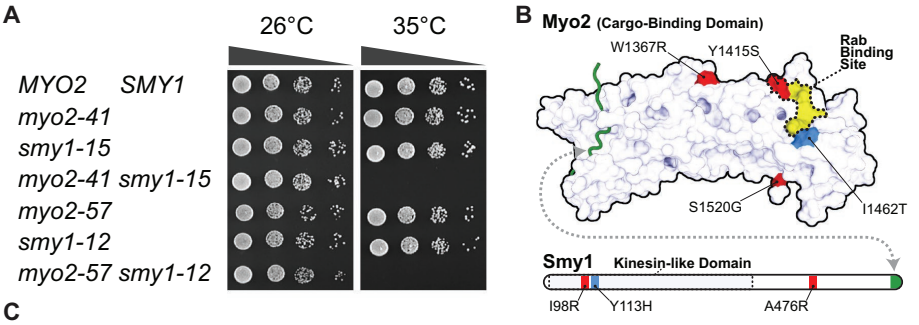

C

Overexpression suppressors of *myo2-41 smy1-15*

Genes	Clones	Description
CMD1	3/25	Calmodulin
CMK1	1/25	Calmodulin-dependent protein kinase
MLC1	3/25	Light chain for Myo2
SEC4	2/25	Secretory Vesicle Rab GTPase
SMY1	1/25	Kinesin-like myosin passenger-protein
SMI1	6/25	Involved in cell wall synthesis regulation
YPT31	8/25	Trans-Golgi Rab GTPase
YPT32	1/25	Trans-Golgi Rab GTPase

Overexpression suppressors of *myo2-57 smy1-12*

Genes	Clones	Description
MLC1	1/8	Light chain for Myo2
YHR182W	1/8	Putative RhoGAP
YPT31	6/8	Trans-Golgi Rab GTPase

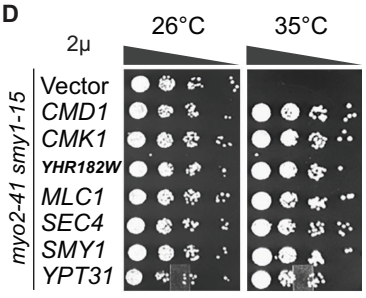

FIGURE 1: Screen for overexpression suppressors of *myo2 smy1* conditional mutants. (A) Growth of the temperature-sensitive strains *myo2-41 smy1-15* and *myo2-57 smy1-12*. Tenfold serial dilutions grown on YPD at either 26°C or 35°C for 2 d. (B) Mutations in *myo2-41 smy1-15* (blue) and *myo2-57 smy1-12* (red) compared with the Myo2-Rab–binding site (yellow/dashed outline) and the Smy1–tail binding site (green). Protein Data Bank: 6IXQ, Tang *et al.*, 2019. (C) Summary table of Gal-overexpression suppressors identified in both strains. (D) Confirmation of overexpression suppression of the identified cDNAs on 2µ vectors in *myo2-41 smy1-15*.

vacuole transport, and Kar9 for association with microtubule plus ends (reviewed in Hammer and Sellers, 2012).

The transport of secretory vesicles by Myo2 is an essential process that has been shown genetically to involve the nonessential kinesin-related protein Smy1 (Lillie and Brown, 1994, 1992). Smy1 interacts directly with Myo2, and we have previously shown that it functions to specifically enhance the association of Myo2 with the secretory vesicle receptor, Sec4 (Lillie and Brown, 1994; Lwin *et al.*, 2016). In this report, we employ a genetic approach to uncover additional components that may be involved in the direct or indirect regulation of secretory vesicle transport. This screen led to the discovery of a previously uncharacterized F-BAR (Fes/CIP4 homology-Bin-Amphiphysin-Rvs protein)-containing RhoGAP (GTPase-activating protein), which we named Rgd3, that regulates Rho3 and Cdc42. Interestingly, Rgd3 associates with vesicles polarized to sites of growth that are distinct from constitutive secretory vesicles. Furthermore, the polarity of Rgd3 vesicles is dependent on an intact actin cytoskeleton. Our study shows that Rgd3 is capable of redistributing Rho3 on the plasma membrane and contributes to overall cell morphology, particularly in cells where polarity is compromised.

RESULTS

Identification of genes whose overexpression suppresses conditional *myo2 smy1* mutants

An essential function of the yeast myosin-V motor encoded by *MYO2* is to transport secretory vesicles to the site of cell growth (Johnston *et al.*, 1991; Schott *et al.*, 1999). The kinesin-related protein Smy1 functions with Myo2 to enhance the association of Myo2 with its receptor on secretory vesicles, the Rab Sec4 (Lillie and Brown, 1994; Beningo *et al.*, 2000; Lwin *et al.*, 2016). We have described *myo2* mutant alleles partially compromised in binding Sec4 in which *SMY1* becomes essential and used these alleles to generate *myo2 smy1* conditional mutations (Figure 1, A and B). To explore what ancillary factors might function directly or indirectly in this process, we used two different *myo2 smy1* strains to screen our regulated *GAL1*-cDNA overexpression library (Liu *et al.*, 1992) for clones that could suppress the temperature sensitivity at 35°C. After isolating and retesting the plasmids from about 250,000 total transformants, 25 clones were recovered and sequenced to yield cDNAs from nine different genes (Figure 1C). Among the cDNAs recovered were *SMY1* itself; genes encoding the Rab proteins Sec4 and Ypt31/32, both of which interact with the cargo-binding domain of Myo2 (Lipatova *et al.*, 2008; Santiago-Tirado *et al.*, 2011); and genes encoding Cmd1 and Mlc1, both of which associate with the lever arm of Myo2 (Brockerhoff *et al.*, 1994; Stevens and Davis, 1998). In addition, we recovered an uncharacterized gene, *YHR182W*, that has a putative RhoGAP domain, and *SMI1* (aka *KNR4*), that has been proposed to play a role in the regulation of cell wall synthesis (Roumanie *et al.*, 2001; Basmaji *et al.*, 2005). When genomic DNA was recovered to express the genes from their own promoters on high-copy 2µ plasmids, the identified genes all suppressed the conditional growth defect of *myo2-41 smy1-15* at 35°C (Figure 1D). However, only four–*YHR182W, MLC1, SMY1,* and *YPT31*—suppressed *myo2-57 smy1-12*, presumably due to the more severe mutation within the Rab-binding site in the Myo2-cargo–binding domain (Figure 1B and Supplemental Figure S1A).

YHR182W, now *RGD3*, encodes a RhoGAP for Rho3 and Cdc42

Previous studies have identified nine RhoGAP proteins in yeast, Bem2, Bem3, Bag7, Lrg1, Sac7, Rgd1, Rgd2, Rga1, and Rga2. *YHR182W* represents one of two additional genes (the other being *ECM25*) whose protein products were computationally predicted to have RhoGAP activity (Roumanie *et al.*, 2001). By sequence analysis, *YHR182W* is most closely related to *RGD1* and *RGD2* (about 15% identity, 25% similarity); thus, for consistency, we decided to name this third relative *RGD3*. All three protein sequences were subjected to HHpred homology detection and found to have a putative N-terminal F-BAR domain and a C-terminal GAP domain (Zimmermann *et al.*, 2018). Rgd2 and Rgd3 also have a DEP (Dishevelled, Egl-10, Pleckstrin-homology) domain–generally involved in membrane targeting and G-protein signaling (Wong *et al.*, 2000; Burchett, 2002)–embedded in the F-BAR domain (Figure 2A). The putative F-BAR and DEP domains of Rgd3 were not previously identified or annotated within the Pfam or SMART databases. These three are the only RhoGAP proteins in *Saccharomyces cerevisiae* with F-BAR domains and together appear to be distantly structurally related to human protein GMIP and the slit-robo family of GAPs.

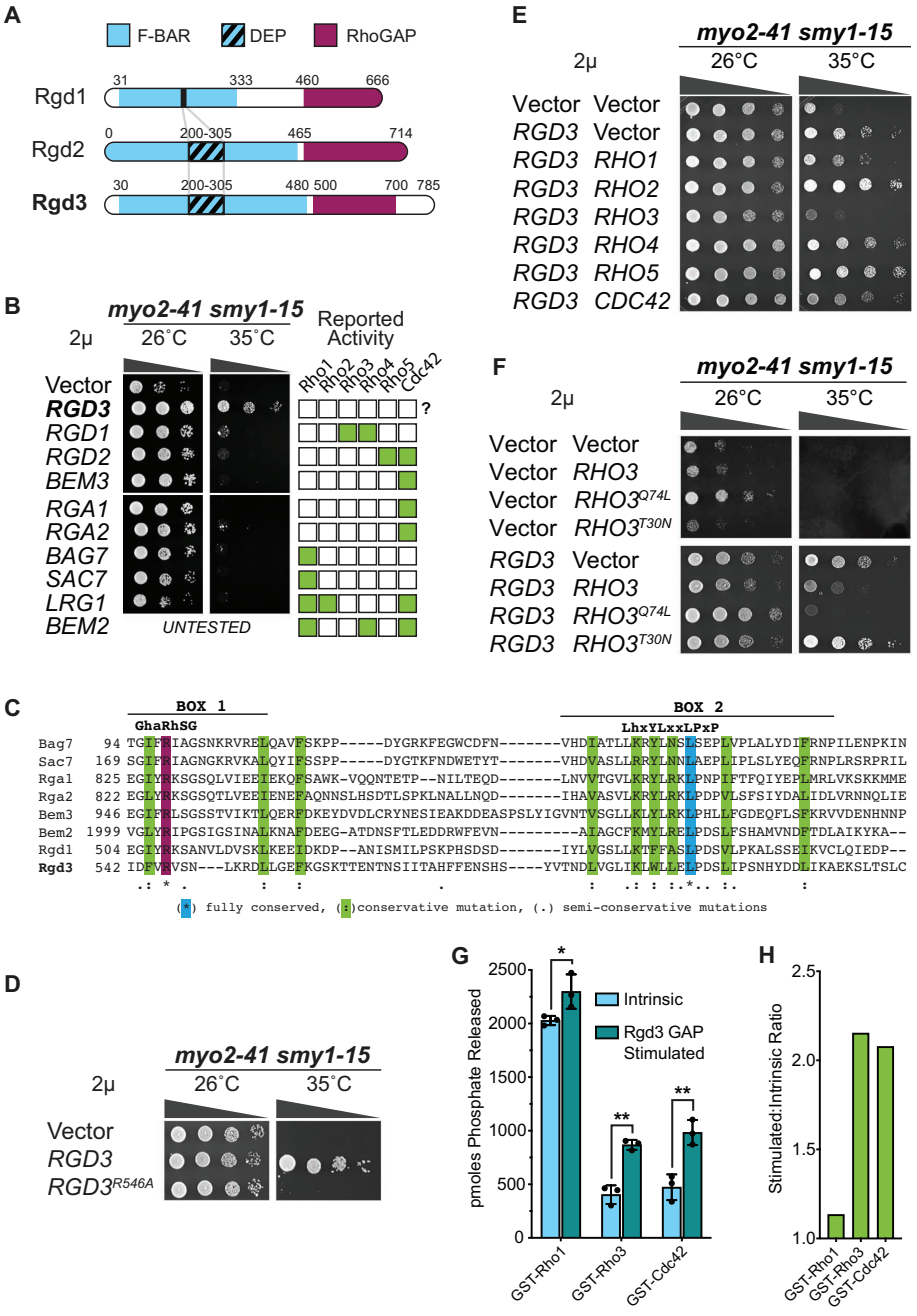

FIGURE 2: Rgd3 (*YHR182W*) is a RhoGAP for Rho3 and Cdc42. (A) Schematic diagram of domains in Rgd3 and related RhoGAPs in *S. cerevisiae* as determined by HHPred. (B) Rgd3 is the only RhoGAP that suppresses *myo2-41 smy1-15* temperature sensitivity. Activities reported in the literature are shown alongside. (C) Alignment of the Rgd3 RhoGAP active site with other known RhoGAPs in *S. cerevisiae*. (D) An arginine residue that aligns with other known catalytic arginine-finger motifs is required for Rgd3's suppression of *myo2-41 smy1-15* temperature sensitivity. (E) Rho3 2µ overexpression exhibits the greatest countersuppression of temperature sensitivity in *myo2-41 smy1-15 2µ RGD3*. Rho proteins were introduced on a second, separate 2µ plasmid. (F) Constitutively active Rho3 ($RHO3^{Q74L}$), and not the inactive form ($RHO3^{T30N}$), exhibits the same countersuppression of Rgd3 suppression seen in F. (G) Rgd3's GAP domain shows greater GAP activity against Rho3 and Cdc42 than Rho1 in a colorimetric malachite green GTPase assay. Three independent assays were performed. *, $p \leq 0.05$; **, $p \leq 0.005$ by Student's *t* test. (H) Ratio of intrinsic GTP hydrolysis to Rgd3-stimulated hydrolysis from G.

To test whether the ability to suppress *myo2-41 smy1-15* is shared by other yeast RhoGAP proteins, we overexpressed eight of the RhoGAPs from their own promoters on 2µ plasmids. Of all the RhoGAPs tested, only *RGD3* overexpression could confer suppression, indicating that it plays a specific role distinct from all the other RhoGAP proteins tested (Figure 2B).

RhoGAP domains have a critical arginine residue that facilitates the hydrolysis of GTP to GDP and Pi (Bourne, 1997). Clustal alignment of Rgd3 with seven yeast RhoGAP proteins identified residue R546 as the critical arginine in Rgd3 (Figure 2C) (Madeira *et al.*, 2019). Overexpression of $RGD3^{R546A}$ failed to suppress the *myo2-41 smy1-15* conditional mutant, showing that GAP activity is necessary for its function in suppression (Figure 2D and Supplemental Figure S2A).

Both genetic and biochemical approaches were used to identify which of the six yeast Rho proteins (Cdc42, Rho1-5) is a substrate for Rgd3. As RhoGAPs are negative regulators of Rho proteins, we also tested whether overexpression of any of the Rho proteins could abolish the ability of *RGD3* overexpression to suppress the conditional *myo2-41 smy1-15* mutant. Rho3 was identified as having the greatest effect, but a lesser effect was also seen with Cdc42 (Figure 2E). The same result was observed in *myo2-57 smy1-12* (Supplemental Figure S1B). The minor decrease in growth for cells containing the *RHO1* 2µ plasmid is not due to countersuppression, but rather is a negative effect of the overexpression of *RHO1* itself (Supplemental Figure S1C).

The ability of *RHO3* overexpression to counteract *RGD3* suppression was dependent on its GTPase activity, as a constitutively active $RHO3^{Q74L}$ had a stronger effect than wild-type *RHO3* or the dominant negative $RHO3^{T30N}$, which showed no effect (Figure 2F).

These genetic data suggest that Rho3, and possibly also Cdc42, are substrates for Rgd3. Of the six Rho proteins, only Cdc42, Rho1, and Rho3 are either essential or nearly essential. We therefore assayed the ability of Rgd3 to stimulate the hydrolysis of GTP by these three Rho proteins loaded with GTP. Under the conditions used, Rgd3 was able to stimulate the GTPase activities of Rho3 and Cdc42 about twofold but had minimal effect on Rho1, which had a higher intrinsic GTP-hydrolysis rate (Figure 2, G and H). Our genetic and biochemical data therefore indicate that Rgd3 is a GAP for Rho3, and likely Cdc42.

Deletion or overexpression of *RGD3* does not confer any growth phenotype in otherwise wild-type yeast (Supplemental Figure S1D). Moreover, it shows no synthetic lethality with *rgd1Δ*, the only other RhoGAP that has been reported to

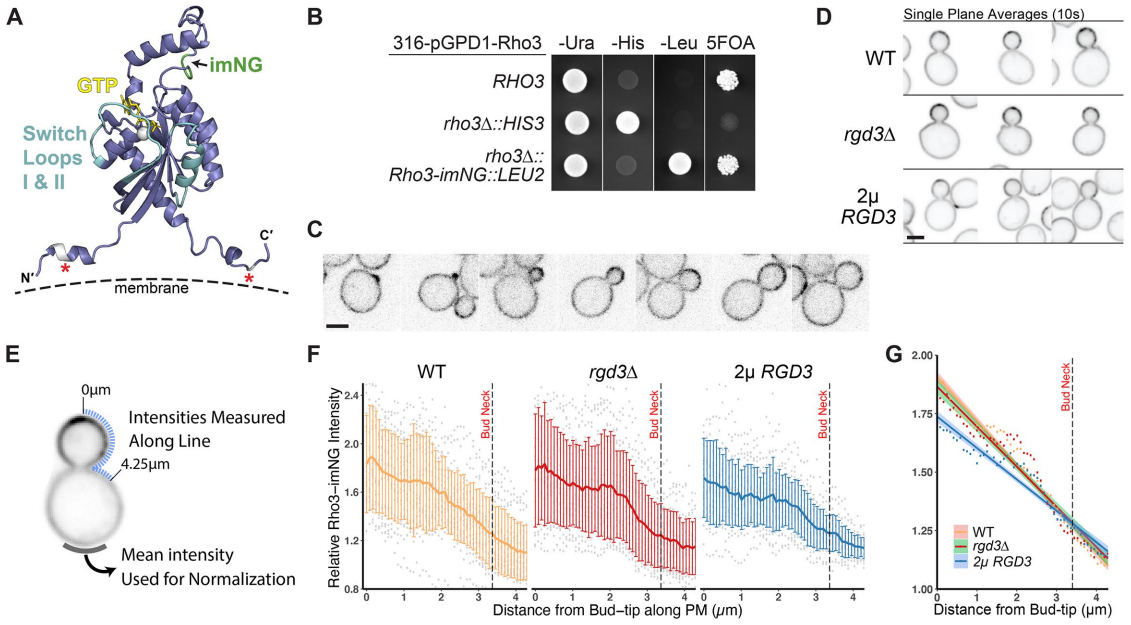

FIGURE 3: Generation of a functional Rho3 fluorescent reporter and effects of Rgd3 on Rho3 localization. (A) Modeled three-dimensional structure of Rho3. Modification of both termini (asterisks) is required for functional Rho3 and membrane localization. mNeonGreen was inserted into a predicted flexible loop on the membrane-distal side of Rho3 (imNG). Structure modeled with Robetta (Song *et al.*, 2013). (B) Rho3-internal-mNeonGreen (imNG) is functional as the sole copy of Rho3 integrated at the endogenous genomic locus. Growth of *rho3::HIS3* or *rho3::Rho3-imNG::LEU2* strains harboring a *URA3-RHO3* plasmid. Eviction of the *URA3* plasmid by selection on 5-Fluoroorotic acid (5-FOA) shows that Rho3-imNG is functional. (C) Rho3-imNG localization in various stages of bud growth; single-plane optical sections. Bar, 2 μm. (D) Examples of Rho3-imNG distribution in response to either deletion or overexpression of *RGD3*. Images displayed are single-plane, cross-sectional averages of 10 s videos. Bar, 2 μm. (E) Schematic representation of the method for measuring distribution and polarity of Rho3-imNG. (F) Raw data (gray) and average distribution of Rho3-imNG intensity (±SD) along the plasma membrane for each genotype. Intensities measured along dashed lines as in E. $n = 23$ per genotype, equal-sized buds chosen. (G) Overlaid linear regression models of data in F ± 95%CI. (Supplemental Video 1 of Rho3-imNG through growth. Maximum projection video time lapse over 3 h. Images taken every 5 min.) (Supplemental Video 2 of Rho3-imNG overexpression shows internal vesicles. Single-plane video. 2μ overexpression is variable, and surrounding cells in this video happened to be lower intensity.)

function with Rho3 (Supplemental Figure S3, A and B). Surprisingly, *rgd3Δ* cells, *rgd1Δ* cells, and *rgd3Δ rgd1Δ* cells all appear to have an unimpaired actin cytoskeleton (Supplemental Figure S3C).

Rgd3 modulates the distribution of Rho3 on the plasma membrane

As Rgd3 is a RhoGAP for Rho3, we wished to localize Rho3 in living cells. It has been notoriously difficult to define the in vivo location of fully functional Rho proteins by tagging, as the small GTPases are C-terminally prenylated and occasionally N-terminally palmitoylated (Ren *et al.*, 2008; Wu and Brennwald, 2010). Rho3 is an example that is modified at both termini, precluding traditional methods of fluorescence tagging. For this reason, Rho3 has been localized by immunofluorescence (Wu and Brennwald, 2010), but no functionally tagged version has been described. We therefore assessed the effect of inserting fluorescent proteins internally at several locations. In just one case, Rho3 was functional when mNeonGreen was inserted into a predicted flexible loop distal to the membrane-binding surface (Figure 3, A and B). This allowed us to explore the location of Rho3 in living cells.

Rho3 internal-mNeonGreen (Rho3-imNG) is predominantly localized to the plasma membrane and enriched at the bud tip (Figure 3C). Enrichment at the bud tip remains through midsized buds and slowly becomes more evenly distributed in larger buds. Rho3 signal then briefly polarizes to the bud neck just before cytokinesis, after which Rho3 localization fluctuates and repolarizes to the membrane proximal to the bud scar, restarting the cycle (Supplemental Video 1). During growth, short-lived patches of increased Rho3 concentration can be seen on the plasma membrane, but we did not explore the nature of this phenomenon. While Rho3-imNG could not be visualized on single vesicles when expressed from its endogenous promoter within the genome, overexpression of Rho3-imNG from the strong *GPD1* promoter showed many vesicles, consistent with earlier immunofluorescence studies (Supplemental Video 2; Robinson *et al.*, 1999).

To quantitate the overall distribution of Rho3 on the plasma membrane, we performed line scan measurements of the fluorescence intensity along the membrane in medium-sized buds (bud diameter 2.07 ± 0.13 μm) from the bud tip to just past the bud neck over a distance of 4.25 μm. The curves were normalized to the mean intensity at the distal region of the mother cells (Figure 3E). This analysis revealed a relatively smooth gradient from the peak intensity at the bud tip decreasing toward the baseline intensity of the mother. This distribution was not significantly affected in *rgd3Δ* cells but was shallower in cells overexpressing *RGD3* (Figure 3, D, F, and G). Though not quantified, representative images of Rho3-imNG in cells with nascent and late buds and in cells where *RGD3* has been either deleted or overexpressed are provided in Supplemental Figure S4. These findings indicate that Rgd3 can influence the distribution of Rho3 and support the contention that it functions as a GAP for Rho3.

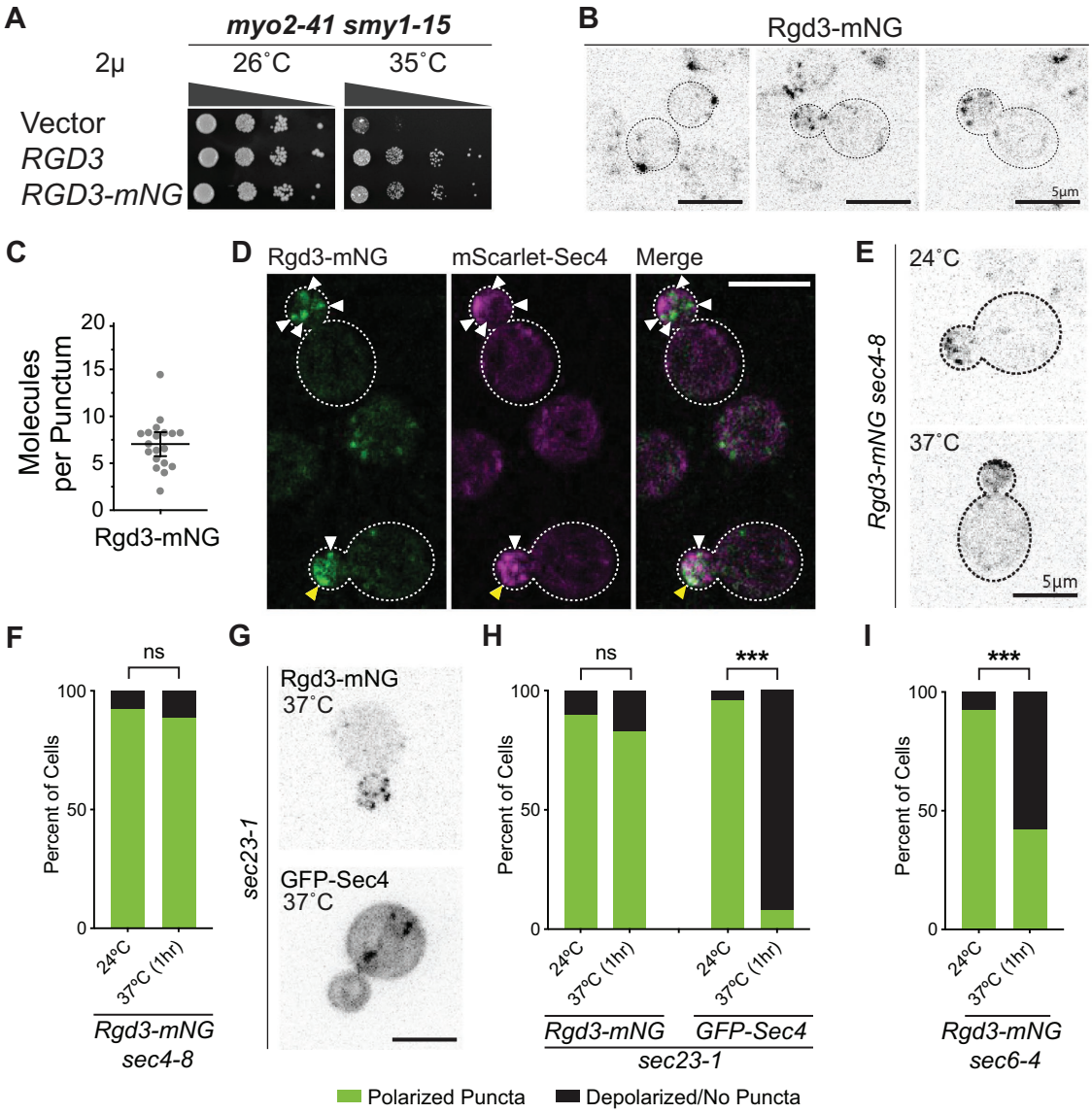

FIGURE 4: Rgd3 localizes to polarized cytosolic puncta independent of a functional secretory pathway. (A) Rgd3-mNG is functional in suppression of *myo2-41 smy1-15* temperature sensitivity. (B) Endogenously tagged Rgd3-mNG localizes to polarized puncta. (C) An average of 7 ± 3 Rgd3-mNG molecules are present per punctum ($n = 19$). (D) Single puncta of Rgd3-mNG (white arrows) and mScarlet-Sec4 do not colocalize, although coincidental overlap may occur near the membrane (yellow arrow). (E) Rgd3-mNG puncta remain polarized in cells where secretory vesicles are depolarized (*sec4-8* cells at 37°C for 1 h). (F) Quantification of the presence of polarized Rgd3-mNG in *sec4-8* cells. (G) Rgd3-mNG puncta remain polarized, while GFP-Sec4 vesicles are abrogated, in cells where the early secretory pathway is blocked (*sec23-1* cells at 37°C for 1 h). (H) Quantification of the presence of polarized Rgd3-mNG and GFP-Sec4 puncta/vesicles in *sec23-1* cells. (I) Quantification of Rgd3-mNG localization in *sec6-4* cells. All quantifications include $n \geq 100$ cells per condition. ***, $p \leq 0.001$ by *z* test for two population proportions. Bars, 5 µm. (Supplemental Video 3 of Rgd3-mNG.) (Supplemental Video 4 of fixed Rgd3-mNG mScarlet-Sec4.)

Rgd3 localizes to polarized puncta distinct from secretory vesicles

Given Rho3's prominent localization to the plasma membrane, we next wanted to see whether Rgd3 appeared to colocalize with it. Rgd3 tagged C-terminally with mNeonGreen (Rgd3-mNG) is functional, as its overexpression can suppress the conditional *myo2-41 smy1-15* mutant (Figure 4A), thereby allowing us to determine the localization of Rgd3-mNG expressed from its chromosomal locus. In vivo imaging revealed dynamic and polarized Rgd3-mNG puncta that were highly concentrated in small budded cells, more distinct in larger budded cells, and often closely associated with the plasma membrane (Figure 4B; Supplemental Video 3). Imaging the puncta is challenging, as we estimate, on the basis of the fluorescence standard Cse4-mNG, that each punctum contains about seven molecules of Rgd3-mNG (Figure 4C). Because of limitations imposed by imaging, we cannot determine the lifetime of the Rgd3 puncta, but we suspect they are very short-lived, probably just a few seconds.

The polarized puncta initially appear very similar to diffusely moving secretory vesicles, so we coimaged Rgd3-mNG and mScarlet-Sec4 and found that the two proteins rarely appeared to colocalize on single puncta (Figure 4D). This exclusivity was further

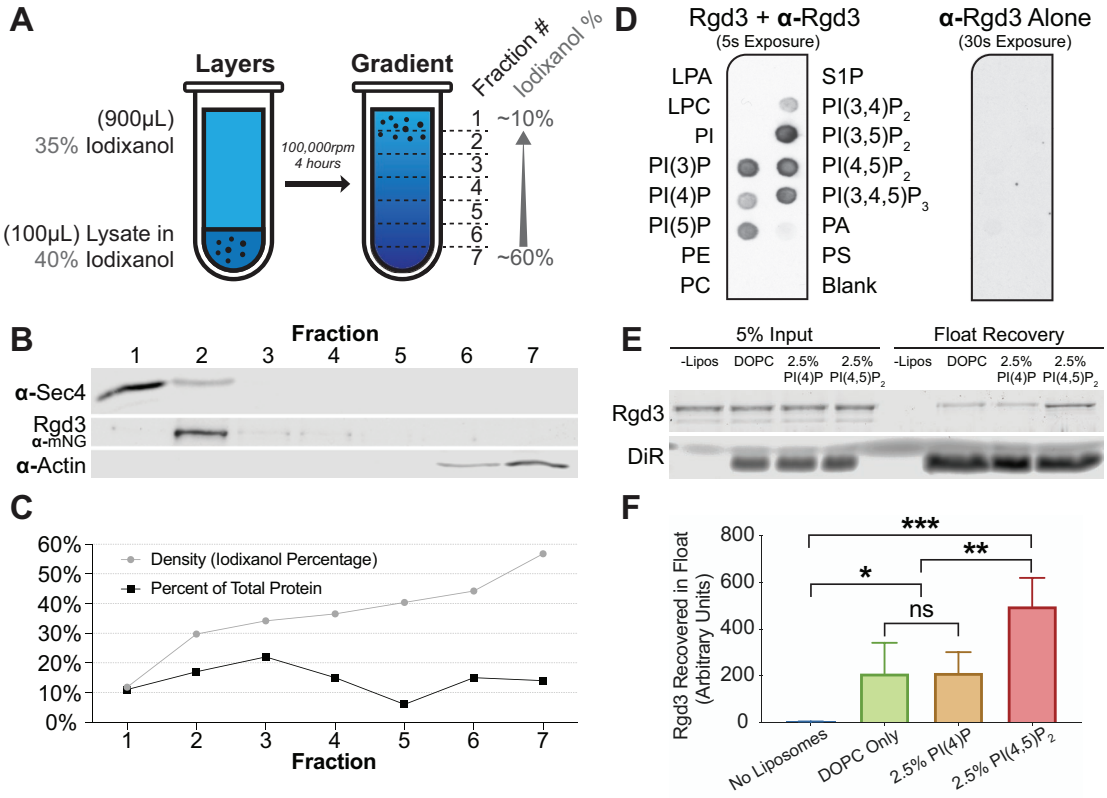

FIGURE 5: Rgd3 associates with vesicles and binds membranes through PIPs. (A) Schematic representation of the iodixanol membrane floatation experiment. (B) Rgd3-mNG floats to a denser fraction than the majority of Sec4 vesicles in a self-forming iodixanol gradient. Representative of four gradients. (C) Iodixanol percentage (gray) and percent of total protein (black) for each fraction from the above experiment. (D) PIP Strip incubated with 1 µg/ml Rgd3 and blotted with rabbit anti-Rgd3. Control strip incubated only with rabbit anti-Rgd3. (E) Coomassie of liposome-bound Rgd3 from a representative liposome flotation assay. Prepared liposomes contain either DOPC alone, DOPC with 2.5% mol PI(4)P, or DOPC with 2.5% mol PI(4,5)P_2. Liposomes were labeled with 1% mol DiR dye. (F) Quantification of Rgd3 recovery in liposome flotation assays. Results from five experiments displayed as mean ± SD. *, $p \leq 0.05$; **, $p \leq 0.005$; ***, $p \leq 0.001$.

confirmed with fixed cells (Supplemental Video 4). Thus, the Rgd3 puncta are either a small subset of traditional secretory vesicles or entirely distinct from them. To test whether these puncta are dependent on secretory vesicles, we examined the location of Rgd3-mNG in two conditional mutants that result in either secretory vesicle depolarization (*sec4-8*; Salminen and Novick, 1987) or loss of secretory vesicles by imposing an early secretory block from the endoplasmic reticulum (*sec23-1*; Kaiser and Schekman, 1990). After *sec4-8* cells were shifted to their restrictive temperature for 1 h, Rgd3-mNG was still present in polarized puncta, indicating that polarized secretory vesicles are not necessary for the polarization of Rgd3 puncta (Figure 4, E and F). In *sec23-1* cells, upon being shifted to the restrictive temperature, Rgd3-mNG again remained in polarized puncta, whereas GFP-Sec4, as a secretory vesicle marker, was no longer visible on discrete vesicles (Figure 4, G and H). We also examined the localization of Rgd3-mNG in *sec6-4* cells that have a conditional defect in secretory vesicle–plasma membrane tethering. In these cells, upon being shifted to the restrictive temperature, secretory vesicles are known to accumulate heavily in the bud. Somewhat confoundingly, Rgd3-mNG puncta became moderately less polarized or disappeared altogether (Figure 4I). Collectively, the data reveal that Rgd3 is not located on constitutive secretory vesicles and its polarized distribution is not directly dependent on the secretory pathway.

Rgd3 associates directly with membranes

The punctate nature of Rgd3's distribution suggests that it may be associated with membranes. Lysates of cells expressing Rgd3-mNG were fractionated on self-forming iodixanol density gradients, a technique developed to separate distinct membrane compartments and previously used to show RabGAP association with membranes (Figure 5A) (Du and Novick, 2001). In these gradients, while Rgd3 floated to a low-density position that indicates vesicle association, this position was repeatedly at a higher density than the majority of secretory vesicles marked by Sec4 (Figure 5, B and C). Thus, Rgd3 appears to be membrane associated and on a vesicular compartment largely, or completely, distinct from secretory vesicles.

Rgd3 has a predicted F-BAR domain, a structure that generally facilitates direct association with membranes through recognition of phosphatidylinositol-containing lipids (reviewed in Ahmed *et al.*, 2010). As an initial test, full-length Rgd3 was expressed in and purified from bacteria (Supplemental Figure S6), and its ability to associate with specific lipids was tested by blotting on "PIP Strips." This revealed a preferential association of Rgd3 with PI(4,5)P_2 or PI(3,5)P_2 and various degrees of affinity for other phosphatidylinositol-phosphate species (Figure 5D). This lipid association was not simply due to negative charge, as no binding to phosphatidylserine was observed. Given its polarized distribution near the plasma

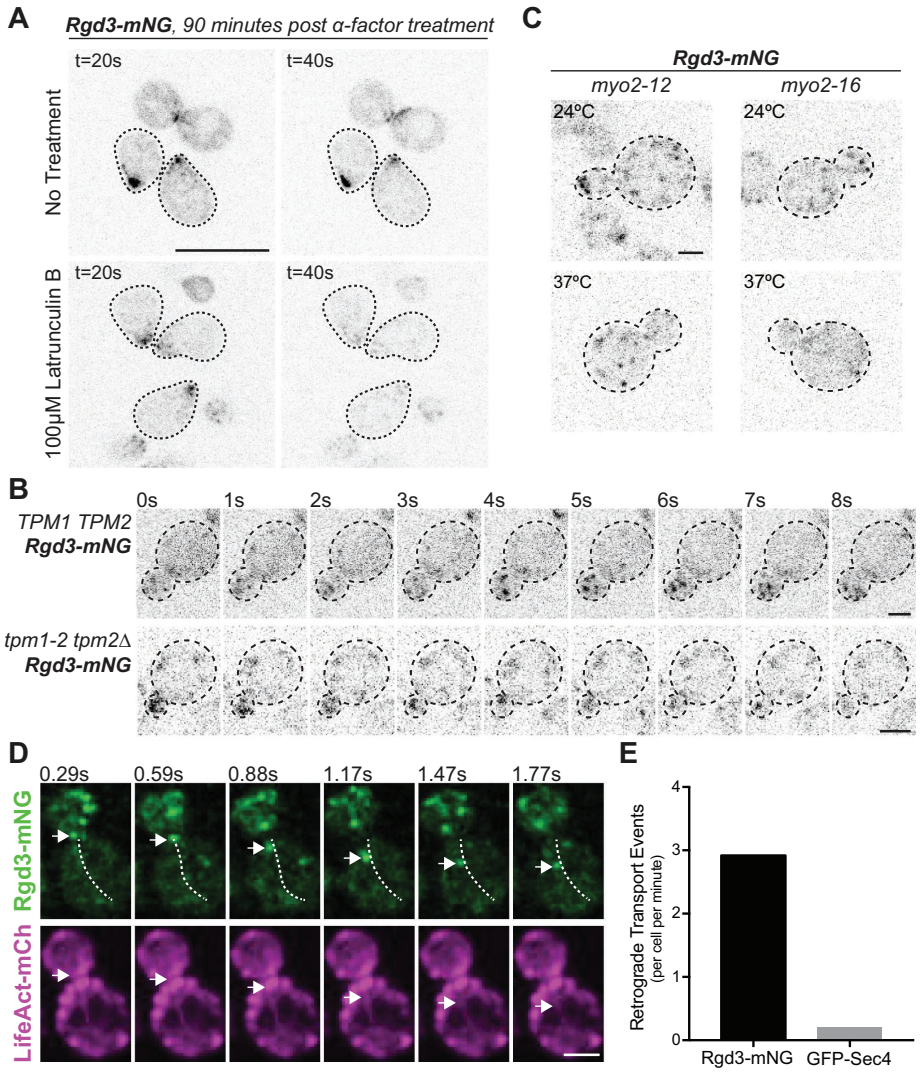

FIGURE 6: Rgd3 vesicle localization and directed movement is actomyosin dependent. (A) Rgd3 vesicles, which are highly polarized in alpha-factor–induced shmooing cells, are rapidly depolarized following actin filament depolymerization (100 mM latrunculin B). Images have been equally adjusted for the intense signal at the shmoo tip; diffuse single vesicles are washed out. Bar, 10 μm. (B) Rgd3 vesicles depolarize following the destabilization of actin cables. *Rgd3-mNG* or *Rgd3-mNG tpm1-2 tpm2Δ* cells were incubated at room temperature and rapidly shifted to a restrictive temperature of 37°C while on the microscope. Imaging began ($t = 0$ s) approximately 45 s after shift to allow adjustment of optics. Bar, 2 μm. (C) *myo2*^{ts} alleles interfere with Rgd3 polarization at both permissive and restrictive temperatures. Bar, 2 μm. (D) Rgd3 vesicles are capable of retrograde (white arrow) movement along actin cables. Actin cable seen in LifeAct-mCherry is traced with a dashed line in the Rgd3-mNG channel. Bar, 2 μm. (E) Quantification of retrograde transport frequency for Rgd3 and Sec4 vesicles. Retrograde transport was defined as five consecutive frames of linear motion away from the bud tip. $N \geq 50$ cells per genotype. (Supplemental Video 5 of Rgd3-mNG LifeAct-mCherry.)

membrane, two of the most likely physiologically relevant lipids are PI(4)P and PI(4,5)P_2. We therefore examined whether purified Rgd3 would associate with artificial liposomes and whether its association is influenced by the presence of these regulatory lipids. In floatation assays, Rgd3 associated weakly with 1,2-dioleoyl-*sn*-glycero-3-phosphocholine (DOPC) and 2.5% PI(4)P liposomes, and this association was greatly enhanced by the replacement of PI(4)P with 2.5% PI(4,5)P_2 (Figure 5, E and F). These results mirror the affinities of PI(4)P and PI(4,5)P_2 seen on the PIP Strip, and we conclude that Rgd3 has the ability to bind directly to membranes.

Rgd3 vesicle polarity is dependent on the actin cytoskeleton and Myo2

We next explored whether Rgd3 polarization is dependent on the actin cytoskeleton. Rgd3 is highly polarized in cells induced to shmoo by α-factor treatment, a phenomenon first observed in high-throughput studies (Kraus *et al.*, 2017; Lu *et al.*, 2018). Treatment of shmooing Rgd3-mNG cells with latrunculin B, to depolymerize actin filaments, resulted in complete depolarization of Rgd3-mNG within 40 s (Figure 6A). Depolarization of Rgd3 puncta via latrunculin B treatment could also be observed in nonshmooing, nascent and early budding cells. Rgd3 polarity, therefore, depends on a dynamic aspect of the actin cytoskeleton.

Latrunculin disrupts all actin filament–dependent processes, including endocytosis. To determine whether Rgd3 polarity is dependent on actin cables, we utilized the temperature-sensitive *tpm1-2 tpm2Δ* strain, which rapidly destabilizes actin cables, leaving actin cortical patches unscathed (Pruyne *et al.*, 2004a). Indeed, Rgd3-mNG signal was lost from the bud within ~60 s of shift to the restrictive temperature (Figure 6B).

As Rgd3 was identified in a strain defective in Myo2-dependent secretory vesicle polarization, a functional link between Rgd3 and Myo2 seems likely. To assess this possibility, we observed Rgd3-mNG localization in two *myo2*^{ts} strains, *myo2-12* and *myo2-16*, both of which show a conditional defect in secretory vesicle polarization (Schott *et al.*, 1999). Interestingly, in both of these strains Rgd3 polarity appeared diminished, with more puncta appearing diffuse in the mother cell, even at the permissive temperature (Figure 6C). When raised to the restrictive temperature for 1 h, Rgd3 polarization to the bud tip was abolished in *myo2-12* and punctate localization of Rgd3-mNG appeared completely lost in *myo2-16*. These data suggest that Rgd3 vesicle polarity, and maybe function, is dependent on Myo2.

Live-cell imaging of Rgd3-mNG in cells also expressing the F-actin marker LifeAct-mCherry showed that Rgd3 puncta are highly dynamic and occasionally move in a retrograde direction (Figure 6D; Supplemental Video 5), away from the bud tip and along actin cables, a phenomenon previously observed for the formin Bni1 and occasionally endocytic vesicles (Kaksonen *et al.*, 2005; Buttery *et al.*, 2007). This contrasts with secretory vesicles marked by GFP-Sec4, which almost never move in retrograde (Figure 6E). Since the Rgd3-marked vesicles appear to be unrelated to secretory vesicles, we explored whether they might be downstream of another actin-dependent process, endocytosis.

Rgd3 is not stably associated with endocytic vesicles

Extensive studies have shown that endocytic vesicles are internalized by Arp2/3-dependent assembly of F-actin at cortical sites (Weinberg and Drubin, 2012), a process that can be imaged using Abp1-mCherry (Kaksonen *et al.*, 2003; Shin *et al.*, 2018). Coimaging of Abp1-mCherry and chromosomally tagged Rgd3-mNG revealed largely independent localizations and that Rgd3 vesicles are far more dynamic than endocytic patches (Supplemental Figure S5A; Supplemental Video 6). Since both Abp1-mCherry and Rgd3-mNG are polarized to the bud, some cases of colocalization do occur. Whether these colocalizations are fortuitous or rather represent a short association of Rgd3-mNG with a subset of endocytic events could not be distinguished. Cells compromised for endocytosis show enhanced sensitivity to the toxic arginine analogue canavanine as the arginine permease becomes enriched on the cell surface (Lin *et al.*, 2008). However, no consistent phenotype was observed on canavanine for deletion or overexpression of *RGD3* (Supplemental Figure S5B). Polarized Rgd3 vesicles still appeared in *end3Δ* cells where endocytosis is compromised (Supplemental Figure S5C) though the frequency and distribution often appeared different from those in wild type (unquantified; Supplemental Video 7). Thus, Rgd3 does not associate with forming endocytic vesicles, but Rgd3 vesicles appear affected by a defect in endocytosis, suggesting some type of relationship.

Rgd3 contributes to overall polarity, and its function is regulated by phosphorylation

Absent a clear pathway responsible for the generation of Rgd3 vesicles, we decided to revisit the original *myo2 smy1* mutant. Tagging of the endogenous Rho3 with imNG in *myo2-41 smy1-15* had little to no effect on growth at room temperature and permitted *RGD3* overexpression suppression at 35°C, like the untagged strain (Figure 7A). Fluorescence examination of Rho3-imNG in *myo2-41 smy1-15* cells either overexpressing *RGD3* or containing an empty vector illustrated that Rho3 distribution is largely wild type at 26°C (Figure 7B). Upon shift to 35°C, however, *myo2-41 smy1-15 Rho3-imNG* accumulates cells with unusual Rho3 polarity and gross morphological defects including, but not limited to, buds growing on buds, buds growing in unusual shapes, and nascent buds forming at bud necks prior to cytokinesis (Figure 7B). Under the same conditions, but when *RGD3* was overexpressed, Rho3-imNG appeared normally polarized and fewer than 3% of cells exhibited similar morphological defects (Figure 7C). These results are consistent with a role for Rgd3 in guiding normal Rho3 distribution on the plasma membrane and bud tip, thereby promoting overall cell polarity and growth.

Earlier high-throughput work has shown that Rgd3 contains an SH3-domain–binding motif at its C-terminus capable of being recognized by the SH3-domain containing factors Bbc1, Lsb1, Lsb3, and Ysc84, all of which participate in actin organization in endocytosis (Figure 7D) (Tonikian *et al.*, 2009). Moreover, the serine and threonines flanking the proline residues of this motif have been found to be phosphorylated in a recent yeast whole phosphoproteome analysis (Lanz *et al.*, 2019). We therefore explored the phenotype of cells in which the serine and threonine residues in Rgd3 were mutated to either alanines (AA/AA mutant) to preclude phosphorylation or aspartic and glutamic acids (DE/EE mutant) to mimic phosphorylation.

Overexpression of the AA/AA mutant was able to suppress the *myo2-41 smy1-15* temperature sensitivity even better than the wild-type ST/TT allele, whereas the DE/EE mutant could not suppress at all (Figure 7E). Further, in *rgd3Δ* cells expressing the Rgd3$^{DE/EE}$-mNG mutant, puncta were very poorly polarized and Rgd3 puncta in cells expressing the Rgd3$^{AA/AA}$-mNG mutant were much more highly polarized (Figure 7F). Since the Rgd3-tail phospho state appears to regulate Rgd3 vesicle polarity and Rgd3 vesicle polarization is dependent on actin cables and Myo2 function, we sought to determine whether Rgd3 was capable of activating and polarizing Myo2 from a depolarized state independent of other polarity cues.

In actively budding cells, Sec4-bound secretory vesicles are the most abundant cargo transported by Myo2 (Pruyne *et al.*, 2004b). For this reason, raising temperature-sensitive *sec4-8* strains to the restrictive temperature results in the inability of Sec4 to activate Myo2 for vesicle transport and a corresponding depolarization of both Myo2 and secretory vesicles (Donovan and Bretscher, 2012). If Rgd3 activates Myo2 to promote Rgd3 vesicle polarization, then introduction of excess *Rgd3$^{AA/AA}$* to *sec4-8 Myo2-3mCherry* cells should permit Myo2 polarization at the restrictive temperature.

In fact, this is exactly what was found. Critically, overexpression of *Rgd3$^{DE/EE}$*, the allele that depolarized Rgd3 vesicles, did not exhibit the same polarity-promoting effect on Myo2 as *Rgd3$^{AA/AA}$* (Figure 7G). We conclude that Rgd3 function and localization are negatively regulated by C-terminal phosphorylation.

DISCUSSION

Yeast has six Rho proteins, three of which, Cdc42, Rho1, and Rho3, are essential, or nearly essential. Cdc42 is the master regulator of polarity (Chiou *et al.*, 2017), Rho1 regulates the Protein Kinase C pathway as well as the cell wall integrity and maintenance pathways (Levin, 2005), and Rho3 is involved in actin regulation, the establishment of cell polarity, and exocytosis (Matsui and Toh-E, 1992; Imai *et al.*, 1996; Adamo *et al.*, 1999; Robinson *et al.*, 1999). Rho proteins are negatively regulated by RhoGAPs, and the yeast genome encodes 11 putative RhoGAP proteins, 10 of which have now been described, including Rgd3. There must therefore be significant redundancy among RhoGAP proteins, making it unsurprising that none of them individually performs an essential function.

Three of the RhoGAP proteins, Rgd1, Rgd2, and Rgd3, also contain an F-BAR domain that implies that they likely associate with moderately curved membranes. Rgd1, a RhoGAP for Rho3 and Rho4, has been shown to localize to polarized vesicles consistent with post-Golgi secretory vesicles (Doignon *et al.*, 1999; Lefèbvre *et al.*, 2012). Rgd2, a RhoGAP for Cdc42 and Rho5, localized to the bud tip in a high-throughput genomic screen (Roumanie *et al.*, 2001; Dubreuil *et al.*, 2018). Here we show that Rgd3 is a RhoGAP for Rho3 and Cdc42 and that it is associated with polarized vesicles. We also found that Rgd3 associated with membranes directly in a phosphoinositide-dependent manner.

While a specific function for Rho3 has not yet been defined, it has been implicated in the establishment of cell polarity, and genetic interactions imply a supporting role in exocytosis through interactions with the exocyst complex. Further, Rho3 has been reported to interact with the lever arm of Myo2 (Robinson *et al.*, 1999; Forsmark *et al.*, 2011). The potential importance of this particular interaction is, at present, unknown, since Rho3 has curiously not been detected (by immunofluorescence or mass spectrometry) on secretory vesicles in cells where it is not overexpressed or mutated (Robinson *et al.*, 1999; Forsmark *et al.*, 2011).

As Rgd3 is a RhoGAP for Rho3, we set out to investigate Rho3's in vivo localization. Both N-terminal and C-terminal tagged Rho3 are nonfunctional, so we explored internal sites in the protein and found that placement of a fluorescent protein in a predicted flexible loop of chromosomal Rho3 did not affect growth of the cells. A deeper literature search later found that a similar method of internally tagging Cdc42 was employed in *Schizosaccharomyces pombe*

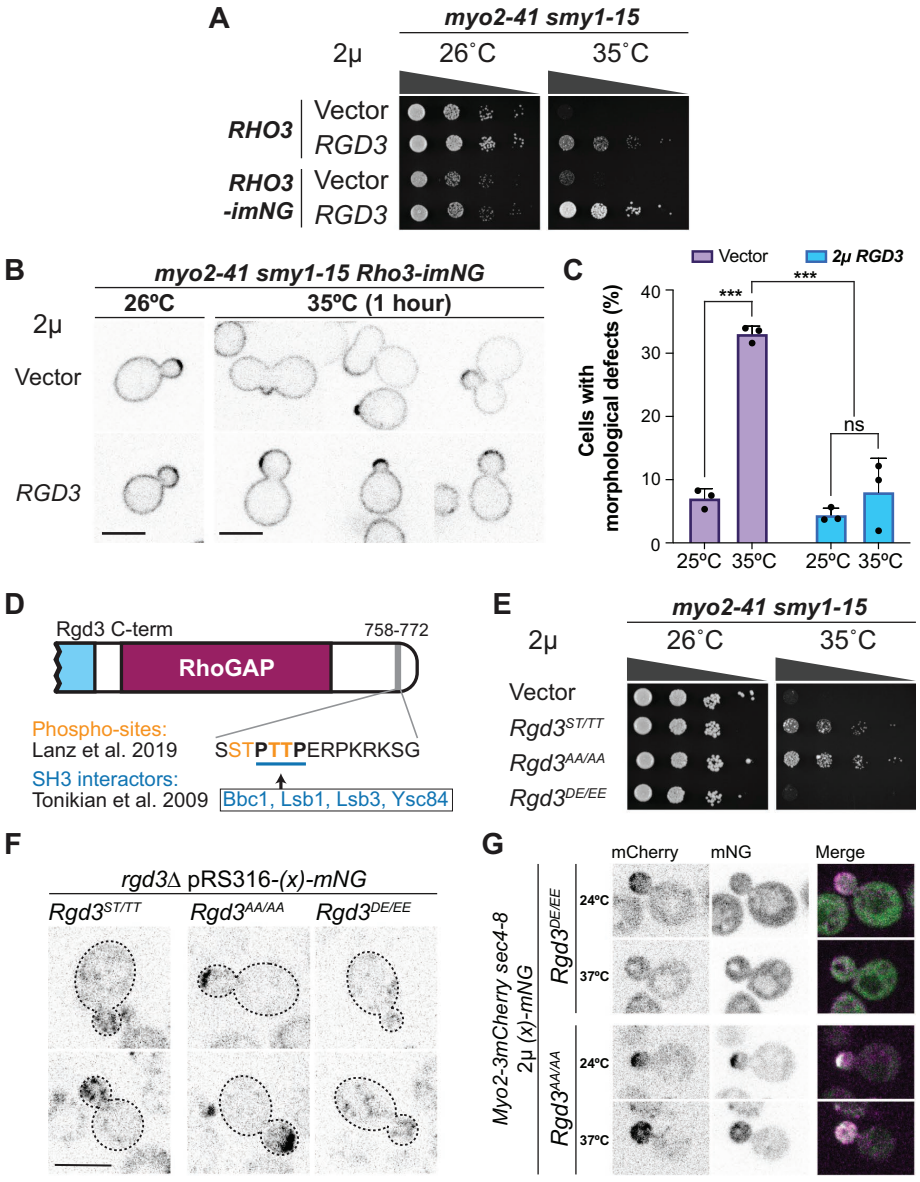

FIGURE 7: Rgd3 is regulated by C-terminal phosphorylation and participates in endocytosis. (A) *RGD3* overexpression is capable of suppressing *myo2-41 smy1-15 Rho3-imNG* temperature sensitivity. (B) *myo2-41 smy1-15 Rho3-imNG* cells exhibit gross morphological defects and mislocalized Rho3 at 35°C that is corrected by overexpression of *RGD3*. (C) Quantification of cells from B. Data from three independent cultures, $n \geq 150$ cells per culture per condition. ***, $p \leq 0.001$ by two-way analysis of variance with Sidak's multiple comparisons test. (D) The tail of Rgd3 contains a motif (bold/underlined) reported to bind SH3 domains, which also contains several phosphorylation sites (orange). (E) The phospho-dead Rgd3 (*Rgd3*$^{AA/AA}$), but not the phospho-mimetic Rgd3 (*Rgd3*$^{DE/EE}$), is capable of rescuing *myo2-41 smy1-15*. (F) Rgd3$^{AA/AA}$-mNG and Rgd3$^{DE/EE}$-mNG mutants localize differently. Bar, 5µm. (G) (*Rgd3*$^{AA/AA}$), but not (*Rgd3*$^{DE/EE}$), is capable of rescuing Myo2 polarity in sec4-8 at the restrictive temperature

(Bendezú *et al.*, 2015). Our Rho3-imNG construct allowed us to establish the in vivo localization of Rho3, which is normally on the plasma membrane in a gradient decreasing from the bud tip toward the mother cell. Further, this gradient is altered in cells overexpressing Rgd3, supporting the notion that it is a regulator of Rho3.

It is believed that Rho3 is always associated with membranes as it has a bidentate membrane association through both termini and it is unable to be extracted by guanosine nucleotide dissociation inhibitor (Tiedje *et al.*, 2008). Perhaps the most astonishing finding with regard to Rho3 localization is that it is not readily observed on secretory vesicles, despite its established role in enhancing secretion. Further, vesicles observed in cells overexpressing Rho3-imNG did not appear to be particularly polarized, as would be expected from Sec4- marked secretory vesicles. The presence of Rho3 on a different, minor class of vesicles may help explain why it was not identified as a constituent of secretory vesicles.

We next endeavored to define the cellular function and localization of Rgd3. Endogenously tagged Rgd3 clearly localizes to short-lived vesicles that are primarily polarized to the growing bud in an actin cable– and Myo2-dependent manner; however, the identity and origin of these vesicles are still unclear. Conditional blocks in secretory vesicle transport (*sec4-8*) and the early secretory pathway (*sec23-1*) had no immediate effect on Rgd3 vesicle abundance or polarity. Reported interactions with the SH3 domain proteins Lsb1, Lsb3, Ysc84, and Bbc1 suggest a role downstream of endocytosis. However, Rgd3 localization appeared to be minimally changed despite the complete block of endocytosis in *end3Δ* cells (Raths *et al.*, 1993; Tuo *et al.*, 2013). That neither blocks of secretion nor endocytosis drastically alter Rgd3 localization suggests that it may reside on vesicles in a step common to both pathways (e.g., transient recycling endosomes) or some other interorganellar transport vesicle.

Although we could not establish a clear, single pathway that Rgd3 participates in, a return to the conditional mutant in which it was identified yielded results that support a role of Rgd3 in regulating Rho3 polarity during growth. Overexpression of *RGD3* in *myo2-41 smy1-15 Rho3-imNG* cells eliminates the apparent defect in Rho3 localization and ensuing overall morphology defects seen in an empty vector control. We further showed that the ability of Rgd3 to suppress *myo2-41 smy1-15*, as well Rgd3 vesicle polarity, is dependent on the phosphorylation state of its SH3-interaction motif.

Collectively our data indicate that 1) Rgd3 vesicles are polarized in a Myo2- and actin cable–dependent manner and also undergo retrograde transport, presumably treadmilling along actin cables; 2) Rgd3 vesicles are not a short-lived intermediate of Sec4-marked secretory vesicles, or a short-lived intermediate of bulk endocytic vesicles; 3) Rgd3 has an F-BAR domain and binds liposomes in a PIP_2-enhanced manner, consistent with originating from the plasma membrane; 4) Rgd3 vesicles contribute to Rho3 distribution on the plasma membrane and morphogenesis in a sensitized background; 5) Rgd3 is negatively regulated by C-terminal phosphorylation; and

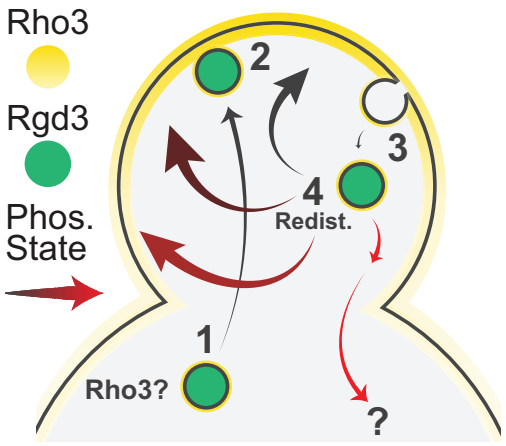

FIGURE 8: Speculative model of Rgd3 function. (1) During polarized growth, hypophosphorylated Rgd3 enables activation of Myo2 and the resulting polarization of Rgd3 vesicles, which likely carry small quantities of Rho3 from the mother cell. (2) Once at sites of growth, Rgd3 vesicles modulate Rho3 localization, potentially by delivery of Rho3 to the membrane via exocyst-dependent fusion. (3) Following inevitable endocytosis of Rho3, whether incidental or stimulated, Rgd3 associates with the vesicles to inactivate the internal pool of Rho3. (4) Phosphorylation state of Rgd3 determines how Rho3 is redistributed, with greater phosphorylation likely being associated with more isotropic growth and a less polarized Rho3 distribution, as seen in large buds. Retrograde vesicles may permit cargo degradation or be a spontaneous occurrence.

6) it contains polyproline motifs that have been shown to bind factors involved in endocytosis.

These properties suggest a speculative model (Figure 8) in which a minor population of regulatory vesicles modulates Rho3 distribution. While we were unable to detect this directly, the simplest explanation for this regulation is that a small population of Rho3 resides on these temporary vesicles, possibly carried internally through endocytosis, where they undergo brief retrograde movement followed by recycling to sites of growth by Myo2. Mutations or backgrounds that result in a large accumulation of Rgd3 vesicles may be needed to test this model fully. It is likely that Rgd3 phosphorylation contributes to its association with the cytoskeletal polarization machinery, so that during highly polarized growth Rgd3 is hypophosphorylated and becomes more phosphorylated as the cell switches to more isotropic growth. As loss of Rgd3 or its overexpression in otherwise wild-type cells has no overt phenotype, testing this model will be challenging and require analysis in genetic backgrounds where its loss causes a strong phenotype.

Our model accounts for why neither complete blockage of endocytosis nor acute blockage of exocytosis abolishes Rgd3 vesicle localization. Furthermore, since unphosphorylated Rgd3 is polarized, overexpression of wild-type Rgd3 would likely result in an increased abundance of unphosphorylated, polarized Rgd3 vesicles. The ability of overexpressed unphosphorylated Rgd3 to polarize Myo2 in the absence of functional secretory vesicles that are its main activator reveals that Rgd3 can directly, or indirectly, activate Myo2. This ability appears to be responsible for suppression of the defects in secretory vesicle transport in the *myo2 smy1* conditionally sensitive strains. As our data suggest that Rgd3 vesicles are distinct from secretory vesicles, Rgd3's effect on secretory vesicle transport as seen in the conditional mutant likely occurs only upon overexpression. Additionally, Rgd3 overexpression might also contribute by indirectly affecting polarity, morphology, or actin dynamics within the bud.

Finally, a potential clue to the cellular function of Rgd3 in the context of a wild-type cell may lie in one of the other interesting suppressors of our original screen, *SMI1*. Smi1 is reported to be involved in cell wall integrity and synthesis regulation as well as various stress responses (Martin-Yken *et al.*, 2003; Basmaji *et al.*, 2005; Yoshikawa *et al.*, 2008). High-throughput studies that included deletion of *YHR182W* imply that Rgd3 may also be involved in stress responses, and microarray studies suggest that *RGD3* expression is regulated downstream of Hog1, Pho85, and filamentous growth (Madhani *et al.*, 1999; Carroll *et al.*, 2001; O'Rourke and Herskowitz, 2004; Yoshikawa *et al.*, 2008). Further studies are necessary to determine the mechanistic details of the pathway(s) in which Rgd3 resides.

MATERIALS AND METHODS

Yeast strains, growth, and transformation

Yeast strains used in this study are listed in Supplemental Table S1. Standard media and techniques for yeast growing and transformation were used. Gene deletion and chromosomal green fluorescent (GFP) tagging were performed by standard PCR-mediated techniques (Longtine *et al.*, 1998). Plasmids from the initial screen were isolated from yeast using a genomic DNA isolation kit (Zymo). Dilution assays were performed by first growing cultures in appropriate media to mid–log phase, diluting all to an OD_{600} of 0.3, and plating 10-fold serial dilutions of this on the indicated plates. All dilution assays were performed three or more times.

cDNA library screening for overexpression suppressors of *myo2 smy1* mutants

One microgram from the GAL1-cDNA library was transformed into an overnight culture (5 ml) (OD_{600} = ~0.8) (Liu *et al.*, 1992). After incubation at 42°C for 45 min, the transformants were washed with dH_2O once, transferred to a 15 ml conical tube, and resuspended in 5 ml of dH_2O. Aliquots (100 µl) were spread on SGal-Ura plates and incubated at 26°C overnight to allow for cDNA expression and then incubated for 5 d at 35°C. In addition, 100 µl of the transformants was spread onto one SC-Ura plate and incubated at 26°C for 5 d to serve as a control for the number of transformants. A total of 80,000 transformants were screened against the *myo2-41 smy1-15* mutant and 150,000 transformants against the *myo2-57 smy1-12* mutant. The plasmids were recovered from the transformants and sequenced to identify the cDNA.

DNA constructs

Plasmids used in this study are listed in Supplemental Table S2. The integrating plasmid pRS306-GFP-Sec4 used to tag Sec4 has been previously described (Donovan and Bretscher, 2012). For constructs utilizing mScarlet, a yeast codon-optimized version of mScarlet (Bindels *et al.*, 2016) was synthesized by Integrated DNA Technologies for downstream PCR amplification and cloning. Centromeric Rho3-imNG plasmids were generated via Gibson assembly, and genomic integration was done by amplification of Rho3-imNG-LEU2 from pRS415-Rho3-imNG plasmids using primers containing homology to the endogenous Rho3 promotor and 3'UTR. Integration and replacement of endogenous Rho3 were verified by PCR. Site-directed mutagenesis of plasmids was performed via inverse PCR using nonoverlapping 5'-phosphorylated primers, one of which contained the intended altered bases at the 5' end. All plasmid and oligonucleotide sequences are available upon request.

Microscopy techniques

All micrographs in the main text were acquired on a CSU-X spinning-disk confocal microscopy system (Yokogawa, Intelligent Imaging Innovations) with a DMI6000B microscope (Leica), 100 × 1.45 NA objective (Leica), and an Evolve 512Delta EMCCD (Photometrics) with a 2× magnifying lens (Yokogawa) for a final resolution of 0.084 µm/pixel. All images and videos shown are transverse, single-plane cross-sections, unless stated otherwise. For live-cell imaging of yeast, cells in mid–log phase were adhered to a glass-bottomed dish (CellVis) coated with concanavalin A (EY laboratories) and washed with the respective cell medium. Molecule counting for Rgd3 was performed by comparison to Cse4 puncta intensity at anaphase, as described previously (Donovan and Bretscher, 2012). Imaging at elevated temperatures was performed in an environmental chamber (Okolab) following 1-h incubations in a 37°C water bath, except for the *tpm1-2 tpm2*Δ experiment, which was performed in a CherryTemp chamber (Cherry Biotech) for rapid temperature shift. Images were analyzed and processed with Slidebook 6.0 software (Intelligent Imaging Innovations) or FIJI. Images and figures were assembled in Illustrator (Adobe).

Yeast two-hybrid constructs and analysis

Full-length Rgd3 (1–785 aa) was fused with the GAL4 activation domain in the pGADT7 vector between *Xma*I and *Xho*I. Each of the Rho proteins (Rho1, Rho2, Rho3, Rho4, Rho5, Cdc42) was fused with the GAL4 DNA binding domain in the pGBKT7 vector between *Xma*I and *Pst*I without their C-terminal CAAX box, to prevent prenylation. The AH109 strain cotransformed with both plasmids was selected in media lacking leucine and tryptophan (SC-2DO: double dropout). Interaction was detected by growth on medium lacking leucine, tryptophan, and histidine (SC-3DO: triple dropout) or SC-3DO + 1 mM 3-aminotriazole.

Purification of GST- and 6His-SUMO–tagged proteins

Fulllength Rho proteins (Rho1, Rho3, and Cdc42) were tagged with GST, while Rgd3, the Rgd3 GAP domain (residues 495–725), and mNeonGreen were tagged with 6His-SUMO. Constructs were expressed in Rosetta 2(DE3) pLysS cells. Cells were grown in terrific broth with antibiotics at 37°C until OD_{600} = ~1.3. A final concentration of 1 mM isopropyl β-D-1-thiogalactopyranoside was added to induce protein expression overnight at 28°C (Rho proteins), for 5 h at 28°C (Rgd3/Rgd3-GAP), or overnight at 18°C (mNeonGreen). GST-Rho proteins were isolated on glutathione beads and eluted with excess glutathione. Bacterially expressed 6His-SUMO fusions were isolated on Ni-NTA resin (Qiagen) and eluted from the resin by direct cleavage of SUMO by Ulp1. Proteins were dialyzed into appropriate assay buffers as necessary.

Antibody production

Rgd3 and mNeonGreen were gel purified following initial SUMO purification and sent to the Pocono Rabbit Farm and Laboratory in Pennsylvania for antibody production. Rabbit antisera against mNeonGreen were affinity purified using mNeonGreen coupled to CnBr beads (MilliporeSigma).

Malachite green GTPase activity assay

GST-Rho proteins were first dialyzed into Rho Protein Buffer (50 mM HEPES, pH 7.5, 100 mM KCl, 1 mM dithiothreitol) to remove excess phosphate and diluted to an equal concentration following a Bradford protein assay. Rgd3-GAP was dialyzed into malachite reaction buffer (50 mM HEPES, pH 7.5, 100 mM KCl, 5 mM EDTA, 10 mM $MgCl_2$). To prepare malachite green reagent, 30 ml of 0.045% (wt/vol) malachite green oxalate (Alfa Aezea #A16186) was combined with 20 ml of 4.2% (wt/vol) ammonium molybdate in 4 M HCl and nutated for 30 min before being filtered through a 0.2 µm filter. Tween 20 was added to 0.02% before use to prevent precipitation.

The malachite green assay for measuring phosphate was described previously (Maehama *et al.*, 2000). In a 96-well plate held on ice, each Rho protein was suspended to a final concentration of 25 µM in nucleotide exchange buffer (50 mM Tris, pH 7.5, 250 mM KCl, 5 mM EDTA, 10 mM $MgCl_2$) with or without 100 µM freshly prepared GTP. Reactions were incubated at 30°C for 30 min before $MgCl_2$ was spiked-in to a final concentration of 10 mM to halt nucleotide exchange. Rgd3-GAP was then added to a final concentration equimolar to that of Rho (for stimulated GTP hydrolysis) or a similar volume of malachite reaction buffer was added (for intrinsic hydrolysis). Reactions were again incubated at 30°C for 30 min. For readout of released phosphate, 100 µl of malachite green reagent was added and allowed to react for 5 min at 37°C. Reactions were equilibrated to room temperature for 5 min before being quickly read for absorbance at 620 nm on a 96-well plate reader. Phosphate released was calculated relative to the absorbance of a simultaneously prepared and read standard curve of sodium phosphate. Three independent reactions were performed with appropriate triplicate controls for each reagent and protein alone.

Measurement of Rho3-imNG distribution

Midsized cells (~2-µm-diameter buds) expressing Rho3-imNG at the endogenous locus were captured in approximately 10 s videos, focused on the bud neck. The resulting frames of each video were averaged in FIJI to yield representative images of Rho3 distributions while minimizing the contributions of temporary punctate structures on the plasma membrane. Freehand lines with a width of 4 pixels were manually drawn from the apparent bud tip (determined by perpendicularity to the bud neck, not signal intensity) through approximately 0.5 µm of the mother membrane. The point of inflection at the bud neck was noted along the intensity profile plot and used for later alignment of the data. Intensity profiles were normalized to the average intensity of an ~0.5 µm stretch of the antipolar membrane in the mother to account for variations in Rho3 expression. Data were analyzed in Open Source R Studio.

Iodixanol gradients and floatation assay

Iodixanol floatation assays were performed essentially as described in Du and Novick (2001), except that gradients were centrifuged in a TLA-100.2 rotor at 100,000 rpm for 4 h. Protein content per fraction was measured via Bradford assay, and iodixanol density was measured via absorbance at 244 nm (Schröder *et al.*, 1997).

Immunoblotting

Samples from iodixanol floatation experiments were resolved by SDS–PAGE, transferred to Immobilon-P membrane (MilliporeSigma), and then blocked for 1 h in 5% milk in TBS-T (0.1% Tween). Membranes were first incubated with primary affinity-purified rabbit anti-mNG and visualized with secondary horseradish peroxidase (HRP)-goat anti-rabbit. Blots were probed again with primary mouse anti-actin (MilliporeSigma) and rabbit anti-Sec4. After being washed, membranes were incubated with secondary AlexaFluor-conjugated goat anti-mouse and donkey anti-rabbit antibodies. Membranes were finally analyzed using the Odyssey infrared imaging system (Li-COR).

PIP Strip

Membranes spotted with 100 pmol of various lipids (PIP Strip; Echelon Biosciences) were blocked overnight at 4°C in blocking

buffer (phosphate-buffered saline [PBS], 0.1% Tween 20, 3% bovine serum albumin). Membranes were incubated at room temperature for 1 h with purified 1 µg/ml full-length Rgd3 in blocking buffer, washed 3× with PBS-T (PBS with 0.1% Tween), and then incubated with rabbit anti-Rgd3 antisera for another hour. Negative controls were performed using PIP Strips that had not been incubated with purified Rgd3 but were also blotted with rabbit anti-Rgd3 antisera. The strips were again washed, incubated with secondary HRP-goat anti-rabbit for 1 h, and visualized on x-ray film with Amersham ECL detection reagents (GE).

Liposome extrusion

Liposomes were generated as previously described (Richardson and Fromme, 2015). Briefly, individual lipid stocks (Avanti Polar Lipids) were combined in 96.5:2.5:1 DOPC:PIP:DiR-dye molar ratios in the presence of chloroform and methanol. Lipid films were vacuum-dried in pear-shaped flasks and rehydrated overnight to 1 mM at 37°C in HK buffer (20 mM HEPES, pH 7.4, and 150 mM KOAc). Lipids were extruded in a miniextruder (Avanti Polar Lipids) with 100-nm filters (Whatman) using 25 passes through the filter. Liposomes were stored at 4°C and were generally used within 1 wk of extrusion.

Discontinuous sucrose density gradient

Liposome floatation assays were performed essentially as previously described (Richardson and Fromme, 2015). For liposome binding, 6 µg of full-length Rgd3 protein was combined with 20 µl of 1 mM liposomes and brought to a final volume of 80 µl in HK buffer. This mixture was allowed to incubate for 1 h at room temperature before being gently, but thoroughly, mixed in 50 µl of 2.5 M sucrose in HK buffer. Unbound protein was separated from liposomes by transferring 100 µl of this mixture to 7 × 20 mm PC ultracentrifuge tubes (Beckman) and carefully layering an equal volume of 0.75 M sucrose buffer followed by 25 µl of sucrose-free HK buffer, and gradients were spun at 100,000 rpm for 20min at 20°C in a TLA-100 ultracentrifuge rotor (Beckman). Top layers were collected, and bound protein was assessed by SDS–PAGE stained with QC Colloidal Coomassie (BioRad). Lipid recovery was normalized to the input samples by measuring relative DiR fluorescence on an Odyssey Imager (Li-COR).

Tetrad dissection

Genetic interaction between *rgd3*Δ and *rgd1*Δ was tested by dissecting tetrads after sporulation. Cells with opposite mating types were grown together overnight at 26°C for mating. Mating efficiency was checked by shmoo projection and zygote formations the next day under the light microscope. Cells were streaked onto diploid-selective plates (SC-Met/-Lys) and single resulting colonies were grown in Yeast Peptone Dextrose overnight, washed with PBS, and resuspended in sporulation media (1% yeast extract, 1% potassium acetate, and 0.05% glucose). Sporulation was carried out over 5–7 d. Once tetrads had formed, 25 µl of zymolyase (stock 1 mg/ml) was added to 50 µl of sporulated cells. The digestion was incubated at 37°C for 6–7 min. Tetrads were dissected using an MSM Singer instrument with a 25 µm fiber needle.

ACKNOWLEDGMENTS

We acknowledge Cornell colleagues Alan Sulpizio for reagents and advice on the malachite green assay, Carolyn M. Highland for assistance on the liposome floatation experiment, and Emr lab members for general advice and reagents. Additional thanks to Riasat Zaman for figure design assistance. This work was supported by National Institutes of Health Grants RO1GM39066 and R35GM131751.

REFERENCES

Adamo JE, Rossi G, Brennwald P (1999). The Rho GTPase Rho3 has a direct role in exocytosis that is distinct from its role in actin polarity. Mol Biol Cell 10, 4121–4133.

Ahmed S, Bu W, Lee RTC, Maurer-Stroh S, Goh WI (2010). F-BAR domain proteins. Commun Integr Biology 3, 116–121.

Basmaji F, Martin-Yken H, Durand F, Dagkessamanskaia A, Pichereaux C, Rossignol M, Francois J (2005). The "interactome" of the Knr4/Smi1, a protein implicated in coordinating cell wall synthesis with bud emergence in Saccharomyces cerevisiae. Mol Genet Genomics 275, 217–230.

Bendezú FO, Vincenzetti V, Vavylonis D, Wyss R, Vogel H, Martin SG (2015). Spontaneous Cdc42 polarization independent of GDI-mediated extraction and actin-based trafficking. PloS Biol 13, e1002097.

Beningo KA, Lillie SH, Brown SS (2000). The yeast kinesin-related protein Smy1p exerts Its effects on the class V myosin Myo2p via a physical interaction. Mol Biol Cell 11, 691–702.

Bindels DS, Haarbosch L, van Weeren L, Postma M, Wiese KE, Mastop M, Aumonier S, Gotthard G, Royant A, Hink MA, Gadella TWJ (2016). mScarlet: a bright monomeric red fluorescent protein for cellular imaging. Nat Methods 14, 53–56.

Bourne HR (1997). The arginine finger strikes again. Nature 389, 673–674.

Brockerhoff S, Stevens R, Davis T (1994). The unconventional myosin, Myo2p, is a calmodulin target at sites of cell growth in Saccharomyces cerevisiae. J Cell Biol 124, 315–323.

Burchett SA (2002). Regulators of G protein signaling. J Neurochem 75, 1335–1351.

Buttery SM, Yoshida S, Pellman D (2007). Yeast formins Bni1 and Bnr1 utilize different modes of cortical interaction during the assembly of actin cables. Mol Biol Cell 18, 1826–1838.

Carroll AS, Bishop AC, DeRisi JL, Shokat KM, O'Shea EK (2001). Chemical inhibition of the Pho85 cyclin-dependent kinase reveals a role in the environmental stress response. Proc Natl Acad Sci USA 98, 12578–12583.

Chiou J, Balasubramanian MK, Lew DJ (2017). Cell polarity in yeast. Annu Rev Cell Dev Biol 33, 77–101.

Doignon F, Weinachter C, Roumanie O, Crouzet M (1999). The yeast Rgd1p is a GTPase activating protein of the Rho3 and Rho4 proteins. FEBS Lett 459, 458–462.

Donovan KW, Bretscher A (2012). Myosin-V Is Activated by Binding Secretory Cargo and Released in Coordination with Rab/Exocyst Function. Dev Cell 23, 769–781.

Du L-L, Novick P (2001). Yeast Rab GTPase-activating protein Gyp1p localizes to the Golgi apparatus and is a negative regulator of Ypt1p. Mol Biol Cell 12, 1215–1226.

Dubreuil B, Sass E, Nadav Y, Heidenreich M, Georgeson JM, Weill U, Duan Y, Meurer M, Schuldiner M, Knop M, Levy ED (2018). YeastRGB: comparing the abundance and localization of yeast proteins across cells and libraries. Nucleic Acids Res 47, D1245–D1249.

Forsmark A, Rossi G, Wadskog I, Brennwald P, Warringer J, Adler L (2011). Quantitative proteomics of yeast post-Golgi vesicles reveals a discriminating role for Sro7p in protein secretion. Traffic 12, 740–753.

Hammer JA, Sellers JR (2012). Walking to work: roles for class V myosins as cargo transporters. Nat Rev Mol Cell Biol 13, 13–26.

Imai J, Toh-e A, Matsui Y (1996). Genetic analysis of the Saccharomyces cerevisiae RHO3 gene, encoding a rho-type small GTPase, provides evidence for a role in bud formation. Genetics 142, 359–369.

Johnston GC, Prendergast JA, Singer RA (1991). The Saccharomyces cerevisiae MYO2 gene encodes an essential myosin for vectorial transport of vesicles. J Cell Biol 113, 539–551.

Kaiser CA, Schekman R (1990). Distinct sets of SEC genes govern transport vesicle formation and fusion early in the secretory pathway. Cell 61, 723–733.

Kaksonen M, Sun Y, Drubin DG (2003). A pathway for association of receptors, adaptors, and actin during endocytic internalization. Cell 115, 475–487.

Kaksonen M, Toret CP, Drubin DG (2005). A modular design for the clathrin- and actin-mediated endocytosis machinery. Cell 123, 305–320.

Kraus OZ, Grys BT, Ba J, Chong Y, Frey BJ, Boone C, Andrews BJ (2017). Automated analysis of high-content microscopy data with deep learning. Mol Syst Biol 13, 924.

Lanz MC, Yugandhar K, Gupta S, Sanford E, Faça V, Vega S, Joiner A, Fromme C, Yu H, Smolka MB (2019). In-depth and 3-dimensional

exploration of the budding yeast phosphoproteome. bioRxiv 700070. doi:10.1101/700070.
Lefèbvre F, Prouzet-Mauléon V, Hugues M, Crouzet M, Vieillemard A, McCusker D, Thoraval D, Doignon F (2012). Secretory pathway-dependent localization of the Saccharomyces cerevisiae Rho GTPase-activating protein Rgd1p at growth sites. Eukaryot Cell 11, 590–600.
Levin DE (2005). Cell wall integrity signaling in Saccharomyces cerevisiae. Microbiol Mol Biol Rev 69, 262–291.
Lillie SH, Brown SS (1992). Suppression of a myosin defect by a kinesin-related gene. Nature 356, 358–361.
Lillie SH, Brown SS (1994). Immunofluorescence localization of the unconventional myosin, Myo2p, and the putative kinesin-related protein, Smy1p, to the same regions of polarized growth in Saccharomyces cerevisiae. J Cell Biol 125, 825–842.
Lin CH, MacGurn JA, Chu T, Stefan CJ, Emr SD (2008). Arrestin-related ubiquitin-ligase adaptors regulate endocytosis and protein turnover at the cell surface. Cell 135, 714–725.
Lipatova Z, Tokarev AA, Jin Y, Mulholland J, Weisman LS, Segev N (2008). Direct interaction between a myosin V motor and the Rab GTPases Ypt31/32 is required for polarized secretion. Mol Biol Cell 19, 4177–4187.
Liu H, Krizek J, Bretscher A (1992). Construction of a GAL1-regulated yeast cDNA expression library and its application to the identification of genes whose overexpression causes lethality in yeast. Genetics 132, 665–673.
Longtine MS, McKenzie A III, Demarini DJ, Shah NG, Wach A, Brachat A, Philippsen P, Pringle JR (1998). Additional modules for versatile and economical PCR-based gene deletion and modification in Saccharomyces cerevisiae. Yeast 14, 953–961.
Lu AX, Chong YT, Hsu IS, Strome B, Handfield L-F, Kraus O, Andrews BJ, Moses AM (2018). Integrating images from multiple microscopy screens reveals diverse patterns of protein subcellular localization change. eLife 7, e31872.
Lwin KM, Li D, Bretscher A (2016). Kinesin-related Smy1 enhances the Rab-dependent association of myosin-V with secretory cargo. Mol Biol Cell 27, 2450–2462.
Madeira F, Park YM, Lee J, Buso N, Gur T, Madhusoodanan N, Basutkar P, Tivey ARN, Potter SC, Finn RD, Lopez R (2019). The EMBL-EBI search and sequence analysis tools APIs in 2019. Nucleic Acids Res 47, W636–W641.
Madhani HD, Galitski T, Lander ES, Fink GR (1999). Effectors of a developmental mitogen-activated protein kinase cascade revealed by expression signatures of signaling mutants. Proc Natl Acad Sci USA 96, 12530–12535.
Maehama T, Taylor GS, Slama JT, Dixon JE (2000). A sensitive assay for phosphoinositide phosphatases. Anal Biochem 279, 248–250.
Martin-Yken H, Dagkessamanskaia A, Basmaji F, Lagorce A, Francois J (2003). The interaction of Slt2 MAP kinase with Knr4 is necessary for signalling through the cell wall integrity pathway in Saccharomyces cerevisiae. Mol Microbiol 49, 23–35.
Matsui Y, Toh-E A (1992). Yeast RHO3 and RHO4 ras superfamily genes are necessary for bud growth, and their defect is suppressed by a high dose of bud formation genes CDC42 and BEM1. Mol Cell Biol 12, 5690–5699.
O'Rourke SM, Herskowitz I (2004). Unique and redundant roles for HOG MAPK pathway components as revealed by whole-genome expression analysis. Mol Biol Cell 15, 532–542.
Pruyne D, Gao L, Bi E, Bretscher A (2004a). Stable and dynamic axes of polarity use distinct formin isoforms in budding yeast. Mol Biol Cell 15, 4971–4989.
Pruyne D, Gao L, Bi E, Bretscher A (2004b). Mechanisms of polarized growth and organelle segregation in yeast. Annu Rev Cell Biol 20, 559–591.
Raths S, Rohrer J, Crausaz F, Riezman H (1993). end3 and end4: two mutants defective in receptor-mediated and fluid-phase endocytosis in Saccharomyces cerevisiae. J Cell Biol 120, 55–65.
Ren J, Wen L, Gao X, Jin C, Xue Y, Yao X (2008). CSS-Palm 2.0: an updated software for palmitoylation sites prediction. Protein Eng Des Sel 21, 639–644.
Richardson BC, Fromme JC (2015). Biochemical methods for studying kinetic regulation of Arf1 activation by Sec7. Methods Cell Biol 130, 101–126.
Robinson NGG, Guo L, Imai J, Toh-e A, Matsui Y, Tamanoi F (1999). Rho3 of Saccharomyces cerevisiae, which regulates the actin cytoskeleton and exocytosis, is a GTPase which interacts with Myo2 and Exo70. Mol Cell Biol 19, 3580–3587.
Roumanie O, Weinachter C, Larrieu I, Crouzet M, Doignon F (2001). Functional characterization of the Bag7, Lrg1 and Rgd2 RhoGAP proteins from Saccharomyces cerevisiae. FEBS Lett 506, 149–156.
Salminen A, Novick PJ (1987). A ras-like protein is required for a post-Golgi event in yeast secretion. Cell 49, 527–538.
Santiago-Tirado FH, Legesse-Miller A, Schott D, Bretscher A (2011). PI4P and Rab Inputs Collaborate in Myosin-V-Dependent Transport of Secretory Compartments in Yeast. Dev Cell 20, 47–59.
Schott D, Ho J, Pruyne D, Bretscher A (1999). The COOH-terminal domain of Myo2p, a yeast myosin V, has a direct role in secretory vesicle targeting. J Cell Biol 147, 791–808.
Schott D, Huffaker T, Bretscher A (2002). Microfilaments and microtubules: the news from yeast. Curr Opin Microbiol 5, 564–574.
Schröder M, Schäfer R, Friedl P (1997). Spectrophotometric determination of iodixanol in subcellular fractions of mammalian cells. Anal Biochem 244, 174–176.
Shin M, van Leeuwen J, Boone C, Bretscher A (2018). Yeast Aim21/Tda2 both regulates free actin by reducing barbed end assembly and forms a complex with Cap1/Cap2 to balance actin assembly between patches and cables. Mol Biol Cell 29, 923–936.
Song Y, DiMaio F, Wang RY-R, Kim D, Miles C, Brunette T, Thompson J, Baker D (2013). High-resolution comparative modeling with RosettaCM. Structure 21, 1735–1742.
Stevens RC, Davis TN (1998). Mlc1p is a light chain for the unconventional myosin Myo2p in Saccharomyces cerevisiae. J Cell Biol 142, 711–722.
Tang K, Li Y, Yu C, Wei Z (2019). Structural mechanism for versatile cargo recognition by the yeast class V myosin Myo2. J Biol Chem 294, 5896–5906.
Tiedje C, Sakwa I, Just U, Höfken T (2008). The Rho GDI Rdi1 regulates Rho GTPases by distinct mechanisms. Mol Biol Cell 19, 2885–2896.
Tonikian R, Xin X, Toret CP, Gfeller D, Landgraf C, Panni S, Paoluzi S, Castagnoli L, Currell B, Seshagiri S, *et al.* (2009). Bayesian modeling of the yeast SH3 domain interactome predicts spatiotemporal dynamics of endocytosis proteins. PLoS Biol 7, e1000218.
Tuo S, Nakashima K, Pringle JR (2013). Role of endocytosis in localization and maintenance of the spatial markers for bud-site selection in yeast. PLoS One 8, e72123.
Weinberg J, Drubin DG (2012). Clathrin-mediated endocytosis in budding yeast. Trends Cell Biol 22, 1–13.
Wong HC, Mao J, Nguyen JT, Srinivas S, Zhang W, Liu B, Li L, Wu D, Zheng J (2000). Structural basis of the recognition of the Dishevelled DEP domain in the Wnt signaling pathway. Nat Struct Biol 7, 1178–1184.
Wu H, Brennwald P (2010). The function of two Rho family GTPases is determined by distinct patterns of cell surface localization. Mol Cell Biol 30, 5207–5217.
Yoshikawa K, Tanaka T, Furusawa C, Nagahisa K, Hirasawa T, Shimizu H (2008). Comprehensive phenotypic analysis for identification of genes affecting growth under ethanol stress in Saccharomyces cerevisiae. FEMS Yeast Res 9, 32–44.
Zimmermann L, Stephens A, Nam S-Z, Rau D, Kübler J, Lozajic M, Gabler F, Söding J, Lupas AN, Alva V (2018). A completely reimplemented MPI bioinformatics toolkit with a New HHpred server at its core. J Mol Biol 430, 2237–2243.